J Low Temp Phys
DOI 10.1007/s10909-014-1125-5

Characterization and Performance of a Kilo-TES Sub-Array for ACTPol

E. A. Grace · J. Beall · H. M. Cho · M. J. Devlin · A. Fox · G. Hilton · J. Hubmayr · K. Irwin · J. Klein · D. Li · M. Lungu · L. B. Newburgh · J. Nibarger · M. D. Niemack · J. McMahon · L. A. Page · C. Pappas · B. L. Schmitt · S. T. Staggs · J. Van Lanen · E. Wollack

Received: 29 July 2013 / Accepted: 30 January 2014

Abstract ACTPol is a polarization-sensitive receiver upgrade to the Atacama Cosmology Telescope (ACT) which will make millimeter wavelength measurements of the small-scale polarization anisotropies of the cosmic microwave background to investigate the properties of inflation, dark energy, dark matter, and neutrinos in the early Universe. ACTPol will employ three arrays of transition edge sensor (TES) bolometer detectors. The detectors, with a target transition temperature of 150 mK, will be operated at a bath temperature of 100 mK provided by a dilution refrigerator. One array operating at a central frequency of 150 GHz and consisting of 1024 TESes achieved first light at the ACT site in July 2013. We anticipate fielding the remainder of the focal plane, consisting of a second 150 GHz array and a multi-chroic array sensitive

E. A. Grace (✉) · L. A. Page · C. Pappas · S. T. Staggs
Department of Physics, Princeton University, Princeton, NJ 08540, USA
e-mail: egrace@princeton.edu

J. Beall · H. M. Cho · A. Fox · G. Hilton · J. Hubmayr · K. Irwin · D. Li · J. Nibarger · J. Van Lanen
National Institute of Standards and Technology, Boulder, CO 80305, USA

M. J. Devlin · J. Klein · M. Lungu · B. L. Schmitt
Physics Department, University of Pennsylvania, Philadelphia, PA 19104, USA

L. B. Newburgh
Dunlap Institute, University of Toronto, 50 St. George St, Toronto, ON M5S 3H4, Canada

M. D. Niemack
Physics Department, Cornell University, 389 Physical Sciences Building, Ithaca, NY 14853, USA

J. McMahon
University of Michigan, 450 Church Street, Ann Arbor, MI 48109, USA

E. Wollack
NASA Goddard Space Flight Center, Greenbelt, MD 20771, USA

Published online: 21 February 2014

to 90 and 150 GHz, at the end of the 2013 observing season. In these proceedings, we present characterization of key detector parameters from measurements performed on the first array both in the lab and during initial field testing. We comment on the design goals, measurements, and uniformity of the detector transition temperatures, saturation powers, and thermal conductivities while detailing measurement methods and results for the detector optical efficiencies and time constants.

Keywords Cosmic microwave background · Transition edge sensor · Bolometer · Polarimetry

1 Introduction

Measurements of the polarized cosmic microwave background (CMB) anisotropies promise to open up new paths to investigate the history and structure of the universe beyond what is possible from measurements of the temperature anisotropies [1]. Because of the faintness of the polarized component of the CMB, these measurements will require large arrays of sensitive, background limited polarimeters. ACTPol [2], a new polarization sensitive receiver for the Atacama Cosmology Telescope (ACT), will employ such arrays to characterize the small scale polarization of the CMB. The ACTPol instrument is composed of the original ACT mirrors [3] and a new cryogenic receiver housing three arrays of $\sim$1000 transition edge sensor (TES) bolometers each. Two of the arrays will have 150 GHz sensitivity and the third targets simultaneous 90 and 150 GHz dichroic sensitivity.

In implementing such large detector arrays, a thorough characterization of the detector properties and behavior is necessary for optimizing the achievable performance of the full focal plane. We present characterization of key detector parameters from the first ACTPol array. This array was deployed to the telescope site in March 2013. Progress on the development and testing of the second two arrays are detailed in other contributions to these proceedings [4,5].

2 Detector and Array Design

Each ACTPol focal plane consists of an array of ortho-mode transducer (OMT) coupled TES bolometers. The OMT is coupled to a waveguide input and a quarterwave backshort cavity [7]. The radiation is fed onto the planar OMT where it is separated into orthogonal polarization components by the opposing pairs of antenna probes [8]. The two components of the polarization signal are carried to their respective TES islands via niobium microstrip line. The power is deposited through the lossy gold meanders on the island which has a weak thermal link to the bath through four silicon nitride legs [9]. The superconducting element of the TES, whose steep resistance versus temperature relationship enables sensitive measurements of this power, is a molybdenum-copper bilayer with a transition temperature tuned to approximately 150 mK. These pixels are fabricated on monolithic three-inch detector wafers at NIST. The first ACTPol array consists of a total of six wafers in two different varieties, three hexagonal wafers (hexes) with 127 pixels each and three semihexagonal wafers (semi-

hexes) with 47 pixels each, for a total of 512 pixels or 1044 TESes in the full array of which 1024 are read out.

3 Laboratory Array Characterization

The first array was assembled and installed in the ACTPol cryostat where a variety of measurements were made to characterize its optical, thermal, and electrical properties. The saturation power ($P_{\rm sat}$) is the power required to drive the TES into its normal state and determines the loading conditions under which the detector can operate. We define the $P_{\rm sat}$ as the bias power at 50 % of the normal resistance (R_n). The $P_{\rm sat}$ of the TES is related to the transition temperature (T_c) and thermal conductance (G) via the following power law [6]:

$$P_{\rm sat} = \kappa (T_c^n - T_b^n), \tag{1}$$

$$G = \frac{d P_{\rm sat}}{dT} = \kappa n T_c^{n-1}. \tag{2}$$

A target $P_{\rm sat}$ of 13.5 pW in the absence of optical loading (P_γ) was selected with the aim to exceed the expected P_γ by a safety factor of three. Under the constraints of a target $P_{\rm sat}$ and bath temperature, a target T_c and G are selected to optimize the thermal noise performance.

The target values selected for ACTPol were T_c = 150 mK and G = 240 pW/K. We measure the detector $P_{\rm sat}$ values by ramping the detector bias and observing the bias power at 50 % R_n. The measured array-averaged $\langle P_{\rm sat} \rangle = 9.4 \pm 3.1$ pW. The T_cs were measured by ramping the bath temperature of the array package and observing the temperature at which the TES was driven normal. We find $\langle T_c \rangle = 147 \pm 7$ mK. By measuring the saturation power of the TES at a range of bath temperatures, Eq. 1 can be fit for the parameters κ and n allowing a measurement of the thermal conductance. This gives the results $\langle \kappa \rangle = 5200 \pm 2400$ pW/K^n and $\langle n \rangle = 3.2 \pm 0.2$ with a resulting $\langle G \rangle = 236 \pm 59$ pW/K.

In our time domain multiplexing read out scheme many detectors are biased on the same bias line placing stringent uniformity requirements on their thermal properties. We achieve sufficient uniformity on the wafer level with the main variation across the array occurring from wafer to wafer, as can be seen in Fig. 1. The average wafer level standard deviations are 3.5, 17, and 11 % for the T_c, $P_{\rm sat}$, and G measurements respectively, sufficient to consistently achieve simultaneous biasing of 96 % of TESes between the cut limits of 10 and 80 % R_n.

In the laboratory environment, a reduced aperture Lyot stop with approximately 5 % spillover efficiency was installed to prevent saturation of the detectors. The optical efficiency of the pixels was measured using aperture-filling blackbody sources at two different temperatures (77 and 293 K) formed from highly emissive Eccosorb foam. Assuming blackbody emission and single-moded coupling of the feedhorn, the expected loading at the detectors is:

$$P_\gamma = \int_{\nu_0}^{\nu_1} \tau(\nu) \frac{h\nu}{e^{\frac{h\nu}{kT}} - 1} d\nu. \tag{3}$$

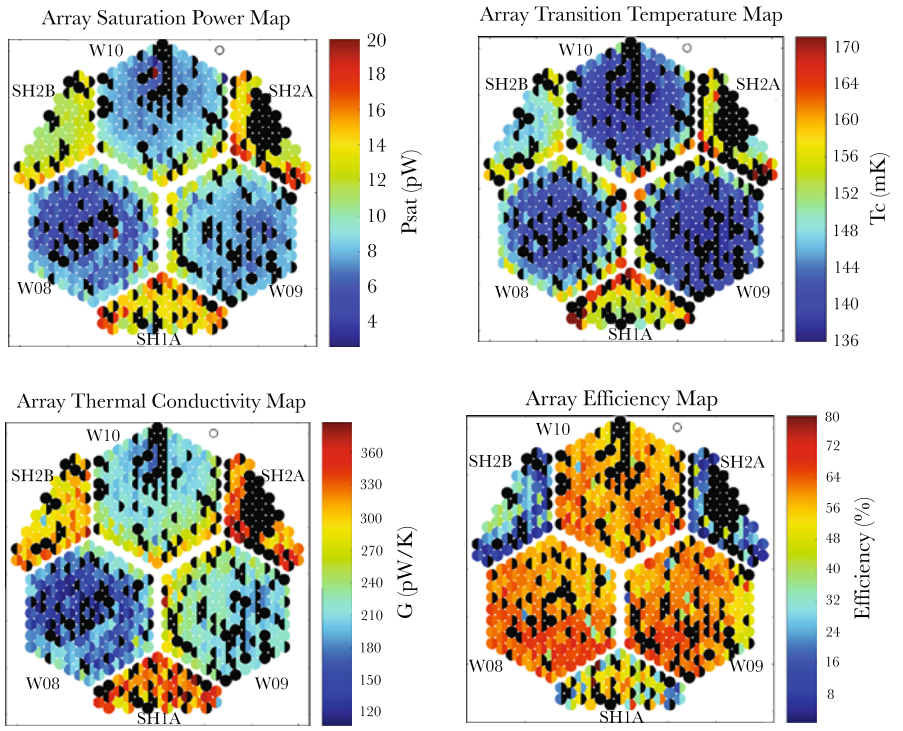

Fig. 1 Maps of measured detector parameters across the array. *Black regions* indicate non-functioning detectors or detectors that are not read out. The parameters are fairly uniform on the wafer level, with the largest differences occurring among wafers. Variation on the wafer occurs in a radial pattern with slightly elevated P_{sat}, T_c, and G values at the very edges of the wafers (Color figure online)

Here ν_0 and ν_1 are the edges of the band which are defined by the low-pass metal mesh filters, which have well-measured transmission characteristics, on the high end and by the waveguide cutoff on the low end. $\tau(\nu)$ is the transmission of the various components in the optical path, including the window, lenses, Lyot stop, and filters. The optical efficiency of the detectors can then be taken as the ratio of the observed power difference over the prediction from Eq. 3:

$$\eta = \frac{P_{\mathrm{sat,77K}} - P_{\mathrm{sat,300K}}}{\Delta P_{\gamma,\mathrm{predicted}}}. \tag{4}$$

We find three tiers of optical efficiency values in the first array wafers - the three hex wafers have ∼60 % efficiency, one of the semihexes has ∼50 % efficiency, and the other two semihexes (which were fabricated on the same wafer) have ∼20 % efficiency. These results have a systematic uncertainty at the level of ∼15 %, dominated by the uncertainty of the load temperatures and the estimation of the Lyot stop transmission. Confirmation of the optical efficiency will be made in the field using observations of planets whose brightnesses are well-calibrated. Because of the observed variation in efficiency, we are monitoring the achieved loss tangents and dielectric constants

Table 1 The measured average ACTPol detector parameter values and detector yield by wafer for the first 150 GHz array as measured in the full receiver

Wafer	Wafer type	Yield (%)	T_c (mK)	$P_{\rm sat}$ (pW)	G (pW/K)	η (%)
W10	Hex	71	143 ± 5	8.4 ± 1.7	226 ± 30	59 ± 5
W09	Hex	71	143 ± 5	8.5 ± 1.6	225 ± 24	61 ± 8
W08	Hex	81	146 ± 6	7.1 ± 1.8	173 ± 33	62 ± 7
SH1A	Semihex	73	158 ± 5	14.4 ± 1.9	326 ± 25	47 ± 14
SH2A	Semihex	80	156 ± 6	14.4 ± 2.1	327 ± 24	18 ± 18
SH2B	Semihex	78	151 ± 4	12.3 ± 1.2	303 ± 19	21 ± 12

of second array detectors carefully (see Pappas et al. [4] for further discussion). A summary of the measured parameter values for the first array can be found in Table 1.

4 Time Constants

The ACTPol receiver and first array were shipped to the site in Chile in March 2013. During an initial cool down performed before installing the receiver on the telescope, an exploration of various methods of measuring the detector time constants was conducted.

Because the time constants low pass filter the data, their measurement provides key input into the scan strategy needed to avoid rolling off the small-scale portion of the signal band. The natural TES thermal time constant depends on the heat capacity (C) of the island and thermal conductance (G) to the bath. In fabrication, the time constants are tuned by adding heat capacity to the TES island in the form of a PdAu thermal mass. For ACTPol, we target an $f_{\rm 3db}$ of at least 50 Hz.

One measurement method uses an optical chopper setup where the detectors are alternately exposed to a reflective metal plate and the sky at frequencies from 5 Hz to 120 Hz. At each frequency we find the power under the peak in the FFT minus the background power spectral density. The falloff of the integrated peak response is fit to a single pole rolloff to find the $f_{\rm 3db}$. We also find time constants by ramping the TES bias in a square wave and measuring the settling time of the TES current. In the time domain, the settling of the current response is fit to an exponential where the exponent is the inverse of the time constant.

The bias step method provides an efficient and repeatable technique for time constant calibration during observing. Because this method does not involve the optical chain, the resulting time constants may differ from the optical time constants. Comparison of the two methods reveals good correlation as shown in Fig. 2. To further our understanding, the time constants will also be measured using planet scans on the telescope.

A more complete electrothermal modeling of the detector response reveals a dependence of the time constant on the bias conditions of the TES [10].

$$f_{\rm 3db} = \frac{G}{2\pi C}\left(1 + \frac{(1-(R_{\rm sh}/R))\alpha}{(1+\beta+(R_{\rm sh}/R))GT_c}P_J\right). \tag{5}$$

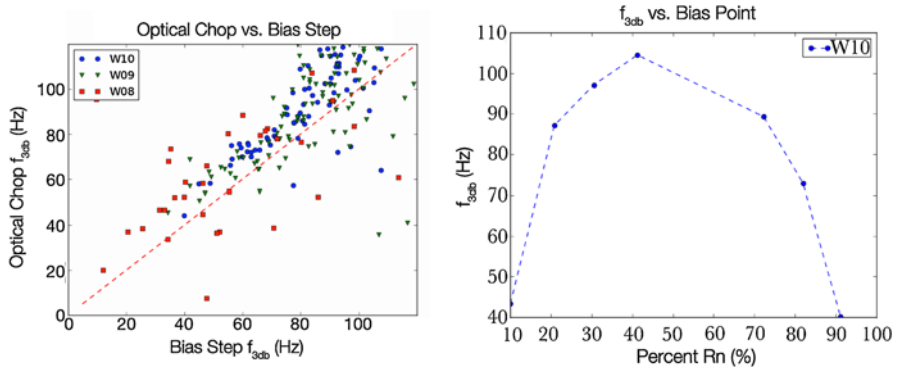

Fig. 2 *Left* A comparison of the measured $f_{3\mathrm{db}}$s using the bias step and optical chop methods for the three hex wafers. The correlation between the two methods is clear although the existence of large deviations for some detectors requires additional investigation. The optical chop method finds slightly faster values than the bias step method. *Right* The average of the wafer W10 $f_{3\mathrm{db}}$s across the transition as measured using the bias step method. The detectors show a fairly constant $f_{3\mathrm{db}}$ through the middle of the transition but slow significantly at the edges (Color figure online)

Here R_{sh} is the shunt resistance used to voltage bias the TES, P_J is the bias power, and α and β are parameters characterizing the shape of the transition [6]. The dependence on α and β causes the $f_{3\mathrm{db}}$ to vary with TES bias point, particularly on the edges of the transition. Our measured $f_{3\mathrm{db}}$ values show the expected behavior. Figure 2 shows that fairly constant $f_{3\mathrm{db}}$s are achieved from 20 % R_n to 80 % R_n before slowing at the highest and lowest bias points. This enables a wide range of bias points while still realizing optimal speed performance.

5 Conclusions

We characterized detector parameters for ACTPol and found adequate accuracy and uniformity of the transition temperature, saturation power, and thermal conductivity. The optical coupling efficiencies of our pixels have been characterized in the laboratory with additional field characterization to occur. We have explored several methods of measuring the detector time constants in the field finding good correlation between the optical chop and bias step methods. Further characterization will be done using planet scan measurements.

Acknowledgments This work was supported by the U.S. National Science Foundation through awards AST-0965625, PHY-0855887 and PHY-1214379. The NIST authors would like to acknowledge the support of the NIST Quantum Initiative. The work of E.A. Grace and B. Schmitt were supported by NASA Office of the Chief Technologists Space Technology Research Fellowship awards. We would like to acknowledge the work of Bert Harrop in the bonding and assembly of the first array.

References

1. A. Balbi, P. Natoli, N. Vittorio, arxiv:astro-ph/0606511 (2006)
2. M.D. Niemack et al., in *Proceedings on SPIE Astronomical Telescopes and Instrumentation* **7741**, 77411S (2010)

3. J.W. Fowler et al., Appl. Opt. **46**(17), 3444–3454 (2007)
4. C. Pappas, et al., in this Special Issue LTD15 in J. Low Temp. Phys.
5. R. Datta, et al., in this Special Issue LTD15 in J. Low Temp. Phys.
6. K.D. Irwin, G.C. Hilton, in *Transition Edge Sensors in Cryogenic Particle Detection*, ed. by C. Enss (Springer-Verlag, Berlin, 2005)
7. E.J. Wollack, J. Phys. Conf. Ser. **155**(012006), 42–50 (2009)
8. J.J. McMahon et al., Proc. LTD **13**, P162 (2009)
9. K.Y. Yoon et al., Proc. LTD **13**, P230 (2009)
10. M.D. Niemack, Towards dark energy: design, development, and preliminary data from ACT, Ph.D. Thesis, Princeton University (2008)